CFD Letters

Journal homepage:
https://semarakilmu.com.my/journals/index.php/CFD_Letters/index
ISSN: 2180-1363

Numerical Simulation of Mass Transport Phenomena on Non-newtonian Magnetohydrodynamics Flow of Blood through a Porous Stenosed Bifurcated Artery

Norliza Mohd Zain[1], Zuhaila Ismail[1,*]

[1] Department of Mathematical Sciences, Faculty of Science, Universiti Teknologi Malaysia (UTM), 81310 Johor Bahru, Johor, Malaysia

ARTICLE INFO

Article history:
Received 4 January 2024
Received in revised form 9 February 2024
Accepted 12 March 2024
Available online 31 August 2024

Keywords:
Mass transfer; Magnetohydrodynamic; Porosity; Overlapping Stenosis; Bifurcated Artery; Galerkin Least-squares

ABSTRACT

The transport of atherogenic molecules across a bifurcated artery under the stenotic conditions are examined in this present work simultaneously with the effects of magnetohydrodynamics and non-Newtonian flow of blood. The streaming blood is characterised as the power law rheological model that pass through a constricted vessel which acts as a porous medium considering that stenosis is developed from the deposition of fatty substance. This abnormal growth of plaque accumulation which deposited at lumen of the mother artery is modelled as an overlapping shaped stenosis and can be categorized as multiple stenoses. The incompressible, steady, laminar and viscous flow of blood is governed by the continuity, Navier-Stokes and convection-diffusion equations coupled with the non-Newtonian constitutive equation. The equations governing such fluid motion with appropriate boundary conditions are then numerically solved by a stabilized form of finite element approach known as Galerkin least-squares method. The computational domain and dependent variables are both being approximated by quadratic triangular element interpolation function of isoparametric formulation. Effects of different fluids characterisation and magnetic field has been validated and show a satisfactory agreement with findings from previous literatures, thus verify the applicability of the developed algorithms. The findings on the contour filled of velocity with streamlines pattern, contour field of shear stress distribution and contour filled of concentration are simulated with varying hemodynamic parameters of magnetic intensity and porosity constant. The simulated findings have revealed that shear-thinning fluid is vulnerable to an increasing extension of cholesterol accumulation, particularly in the downstream region of stenosis. This vulnerability is predominantly observed when the largest flow separating region and lowest luminal mass transfer coincide, especially when accompanied by the highest flow porosity and magnetic source application, as compared to its counterpart.

1. Introduction

As a medium of transportation that carries vital responsibilities to sustain and keep the tissues of the body in great condition by supplying essential nutrients and oxygen to human's cells and body

* *Corresponding author.*
E-mail address: zuhaila@utm.my (Zuhaila Ismail)

https://doi.org/10.37934/cfdl.17.1.90113

tissues, blood as a biological fluid also plays the role of getting rid of waste materials in the blood vessels from human's body. Lipid particles that circulate in the blood in the form of low-density lipoproteins (LDLs) tend to accumulate cholesterol along the arterial wall and are frequently correlated with atherogenicity events. This strong connection between LDL cholesterol deposition with the pathogenesis of atherosclerotic cardiovascular disease, which is known as the number one killer among societies in industrialized world, has spurred numerous kinds of studies on LDL cholesterol level mechanisms of blood in the occurrence of cardiovascular events.

This fact has been verified following the criteria outlined in nine Bradford-Hill epidemiological reports by Schade *et al.,* [1] suggesting the significant contribution of LDL cholesterol in the pathogenesis of atherosclerosis and its subsequent progress. The build-ups of this atherosclerotic lesions in the form of fatty deposition at the arterial wall has caused a reduction in the arterial passage that could restrict the blood circulation through the arteries, which would then lead to the stenosis development [2,3]. Stenosis was portrayed as a multiple typed stenoses in two different investigations conducted by Liu and Liu [2] and Reima *et al.,* [3], since this kind of arterial constriction is preferably found in most medical assessment of patients with cardiovascular diseases. The local luminal mass transport in a straight arterial stenosis was examined by these groups of researchers considering the shape of stenosis as an overlapping [2] and double stenoses [3].

Sites with low and fluctuated wall shear stress, which predominantly occurs around bends, bifurcations, junctions and curvatures in the arterial system, are identified by Sarifuddin *et al.,* [4] as the sites highly predisposed to atherosclerotic formation and certain flow complications in the form of flow recirculation and stagnation. The formation of recirculation zone occurring in the downstream region of stenosis has a tendency to create a new intimal thickening by accumulating the cholesterol on its rear end [4]. These conditions may get worse if large strain of shear stresses and mass transfer rates are exerted near the throat of the stenosis, which directly could disrupt the plaque and promote the thrombosis occurrences that would lead to the total blockage of blood being transported to the brain or the heart [5,6]. These high diffusive fluxes exerted on the wall at several locations in the artery that possess a constriction at a maximum height indicated by Chakravarty and Sen [7] as having large concentration gradient result in low concentration of solute at the wall in comparison to the blood. Findings reported by Sarifuddin *et al.,* [4] and Chakravarty and Sen [7] expressed the considerable impact of stenosis appearance in a bifurcated artery on the distribution of diffusive fluxes of the solute. Several different kinds of studies conducted by Iasiello *et al.,* [8], Hossain and Haque [9] as well as Kumar *et al.,* [10] agreed with this view by considering the formation of atherosclerotic plaque in arterial bifurcation with combined effect of mass transport. The significant impact of the severity of stenoses and Reynolds number on flow velocity and solute concentration was evident in a study conducted by Thirunanasambantham *et al.,* [11], focusing on the mass transport phenomena of non-Newtonian flow of blood through a stenosed bifurcated artery.

The outcomes from extensive analysis carried out by Iasiello *et al.,* [8] on the impacts caused by different kind of rheological models (Newtonian, Carreau-Yasuda, power-law and Carreau) on LDL mass transport through the aorta-iliac bifurcation that possess a porous wall has highlighted the appropriateness of predicting the profiles of LDL concentration by treating the rheological behaviours of blood as a non-Newtonian fluid model primarily at large Reynolds number. In another study, Hossain and Haque [9] studied the dynamic response of LDL concentration through a stenosed bifurcated artery in the presence of magnetic field by describing the characteristics of the streaming blood as a Newtonian chemically reactive fluid. The focus of their study is then extended by Kumar *et al.,* [10] with coupled effect of heat source on the flow of blood through a porous bifurcated artery in the presence of an inclined magnetic field that would be beneficial for the clinical treatment of hypotension and carotid tumour. The combined impacts of magnetic field, chemical reaction, and

heat source parameters on the heat and mass transport mechanisms of non-Newtonian flow of blood, treated as a micropolar fluid model accounting for the microscopic effect due to the local structure and micromotion of the fluid particles, was examined by Khan *et al.,* [12], across a vertical stretching/shrinking sheet. Khan *et al.,* [12] observed that the mass transfer rate occurring at the surface diminishes as the heat source parameter increases, and it is enhanced as the chemical reaction parameter increases.

The negatively charged ions contained in the red blood cells has caused an opposing motion of blood in the presence of magnetic field. The electrical conductivity property of blood that works according to the magnetohydrodynamics (MHD) principle offers many positive medical benefits related to health concerns. For instance, magnetic therapy in sports has been reported by Mwapinga *et al.,* [5] to alleviate pain as well as functioned well in blood flow regulation through his research that works on a chemically reactive blood flow through a single arterial stenosis in the presence of an external magnetic field and body acceleration. The interaction between an induced electric current with an externally applied magnetic field causes the cells to align along their long axis in the direction of the magnetic field. Hence, exposure to an externally applied magnetic field results in opposing motion against the blood flow, generating body forces known as the Lorentz force due to the anisotropic orientation of erythrocytes. This may also result in an increment of blood viscosity [13]. Consequently, the resistive force and the rise in fluid viscosity impede blood movement, decreasing its velocity as the strength of the magnetic field intensity increases [14]. Therefore, MHD principles have demonstrated their utility in preventing and providing rational therapy for arterial diseases characterized by accelerated blood flow, such as hypertension and haemorrhages [15].

The porous nature of the diseased vessel, which consists of pores allow molecules of various sizes to penetrate and pass through the endothelial cells, is realistically relevant in characterizing the local luminal mass transport mechanisms. In consideration that stenosis is formed through the accumulation of fatty substances and the proliferation of connective tissues on the endothelial layers, the pathological condition of a diseased vessel as a porous media should seriously be included in the hemodynamic investigation of blood flow through atherosclerotic vessels accompanied by the transport phenomena of solute concentration. In view of that, the mass transport phenomena which takes place in a single arterial stenosis with porosity effect was described by Saket and Kumar [16] on the basis that the steady convection diffusion process of dissolved oxygen is taken into account. Proper research on the interaction that occurs when blood flows through a porous constricted artery under the presence of wall slip, body acceleration, non-Newtonian and magnetic field effects then was conducted by Nandal *et al.,* [17]. The main highlight from this study involves the slip velocity condition at the permeable wall that was found to be beneficial with the combined effects from body acceleration and magnetic field to effectively regulate blood pressure, necrosis, headaches as well as joints and muscles pain [17]. Previously, Nadeem *et al.,* [18] examined the coupled effects of heat and mass transport on Newtonian biomagnetic fluid of blood flow through a tapered single arterial stenosis that is considered equivalent to a fictitious porous structure. A recent study by Omar *et al.,* [19] on the unsteady Casson fluid through a porous medium in the presence of thermal radiation and chemical reaction highlighted the significant role of porous medium. This contribution leads to a reduction in flow resistance, consequently enhancing the fluid motion.

A more comprehensive study that combined the effects of chemical reaction, thermal radiation, heat source and magnetic field inclination on the unsteady magnetohydrodynamics flow of blood passed through a straight porous arterial stenosis was examined by Omamoke and Amos [20]. Results obtained from the investigation conducted by Amos *et al.,* [6] could assist in predicting the possible outcomes for the treatment of cancerous tumour, hypothermia and hyperthermia through the extension of idea from the prior works by Omamoke and Amos [20] with inclusion of slip velocity and

body acceleration effects. The radiation effect, which helps in forecasting the progress of cancerous tumour treatment, is neglected by Amos *et al.,* [6]. Magnetic field exposure of suitable intensities was reported by Abdullahi *et al.,* [17] through the recent study on the MHD Newtonian blood flow through a porous straight artery subjected to the impacts of heat source, thermal radiation, and chemical reaction and inclined magnetic field as a practical way to cure the low blood pressure disorder by controlling the blood flow rate. In addition, by adjusting the magnetic field exposure on the affected areas to a certain slant angle, the incident of strokes, pain and swelling of the infected site could be reduced [21].

The serious complications that occur in the veins or arteries resulted from the atherosclerotic plaque accumulation may contribute to various kinds of cardiovascular diseases such as myocardial infarction, ischemic stroke as well as low and high blood pressure. Therefore, a realistic and relevant set of mathematical models on mass transport phenomena through an arterial constriction may provide an accurate understanding of the transport of macromolecules with dissolved gases to and through the walls of the artery which are also correlated with the growth and progress assessment of atherogenic processes. The mechanisms of mass transfer through an atherosclerotic artery have been addressed in nearly all works cited here that takes into consideration the other combined impacts of magnetic field and porous nature of the diseased vessel. Despite that, the authors discovered that only a few attempts have focused on the non-Newtonian rheological behaviours of blood passed through the atherosclerotic bifurcated artery. These aspects are definitely essential in order to accurately describe the behaviours of blood through the diseased vessel. Hence, our intention through this work is primarily to fill those gaps by mathematically modelling and examining the coupled effects of mass transport on the magnetohydrodynamics flow of blood through a porous arterial bifurcation with an overlapping shaped arterial constriction at the mother artery. The novelty of this study lies in representing blood behaviour using the non-Newtonian fluid model, specifically the power law model, and considering variations in fluid nature such as shear-thinning, Newtonian, and shear-thickening, denoted by appropriate power law indices. This is significant because previous works have not paid much attention to the mass transportation of blood within the constricted artery characterized as a non-Newtonian model. The findings from this study may assist in predicting the outcome of alternative treatment plans for cardiovascular diseases patients, which in terms of cost offers an economically cheap rate. Many medical diagnostic devices rely on magnetic fields for diagnosing cardiovascular diseases. The findings of this study may offer valuable insights to medical practitioners regarding the therapeutic use of magnetic therapy in managing conditions like hypertension, haemorrhages, and gastric infections. Moreover, surgeons aiming to maintain the desired blood flow rate during surgical procedures could harness the resistive nature of the Lorentzian magnetic body force produced by applying an external magnetic field. Additionally, accurate regulation of blood flow rate measurements, which holds significant interest for clinicians and medical scientists, can be achieved by thoroughly considering the realistic pathological conditions of blood as a porous medium, as investigated in this study.

2. Mathematical Formulation of the Problem

The mathematical model for the problem under consideration is developed following a few assumptions that are inflicted into the flow domain in order to simulate the outcome from this present model realistically, such that

i. The mother artery has an arterial constriction which is symmetrical about the axis of the trunk in the shape of overlapping with a maximum height τ_m which occurs at $d + 2l_0 / 6$

and $d+4l_0/6$. The critical height of an overlapping stenosis, $0.75\tau_m$ is located at $d+l_0/2$ as portrayed in Figure 1.

ii. The arterial bifurcation possesses a finite length, x_{max} with 30º angle of bifurcation, β.

iii. The appropriate curvatures are proposed at the flow divider and lateral junctions of the branch artery to avoid any kind of discontinuity that would lead to either a huge separating flow or its non-existence.

iv. The computational domain and flow are represented by using the two-dimensional Cartesian coordinate system by taking the material point (x,y) where the horizontal x-axis is taken along the axis of the trunk, while the y-axis is taken perpendicularly to the axial flow direction.

v. The wall motions of the outer and inner arterial wall are considered rigid in view of its diseased state which made it less compliant.

vi. The cholesterol deposits on the arterial wall that is portrayed as an atherosclerotic constriction is considered similar to a fictitious porous structure.

vii. The streaming fluid is considered steady, laminar, incompressible, fully developed and non-Newtonian in nature under the influence of an external magnetic field that is applied in a transverse direction.

viii. The motion of blood is characterised as a non-Newtonian fluid by taking into account a different fluid characterisation corresponding to the shear-thinning, Newtonian as well as shear-thickening nature of blood described by the appropriate values of the power law index conditionally as $n<1$, $n=1$ and $n>1$, respectively.

ix. The LDL mass transport within an arterial bifurcation is simulated by individually coupling the mass transport equation with the velocity components.

2.1 Arterial Geometry

The arterial geometry involved in this study is modelled as a porous bifurcated channel that possesses an overlapping shaped stenosis in the parent artery as depicted in Figure 1. The construction of this computational domain is expressed mathematically by Chakravarty *et al.,* [22] and Chakravarty and Mandal [23] for the geometric model of the bifurcated system and vessel constriction, respectively. In Figure 1, the parameters a and r_1 describe the radii for the mother and daughter artery, respectively. Meanwhile, l_0 acts as the arterial constriction's length at a distance d from the origin. The onset and offset of the lateral junction are located, respectively, at the axial distance of x_1 and x_2, while x_3 denotes the apex of the vessel.

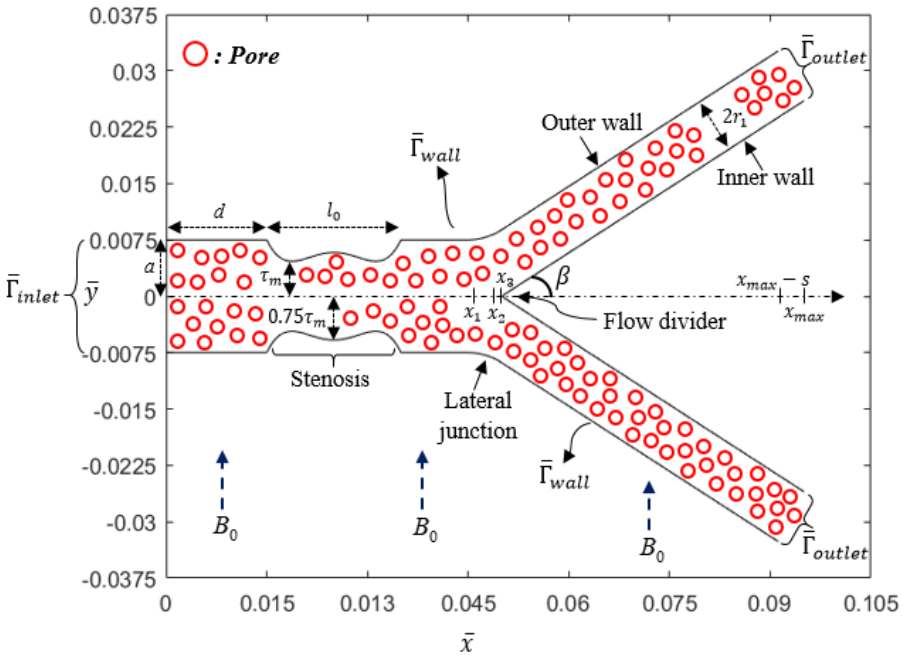

Fig. 1. Schematic diagram of porous bifurcated artery with magnetix flux intensity, B_0 acts in a perpendicular direction of blood flow

2.2 Governing Equations and Boundary Conditions

Based on the specified assumptions, the relevant sets of governing equations for the streaming blood are given as the coupled system of equations comprising of the continuity, Navier-Stokes and convection-diffusion equations, written individually in non-dimensional form as,

$$\frac{\partial u}{\partial x}+\frac{\partial v}{\partial y}=0, \tag{1}$$

$$u\frac{\partial u}{\partial x}+v\frac{\partial u}{\partial y}=-\frac{\partial p}{\partial x}+\frac{\mu_a}{Re}\left[\frac{\partial^2 u}{\partial x^2}+\frac{\partial^2 u}{\partial y^2}\right]-\frac{M^2}{Re}u-\frac{1}{Re\cdot K}u, \tag{2}$$

$$u\frac{\partial v}{\partial x}+v\frac{\partial v}{\partial y}=-\frac{\partial p}{\partial y}+\frac{\mu_a}{Re}\left[\frac{\partial^2 v}{\partial x^2}+\frac{\partial^2 v}{\partial y^2}\right]-\frac{1}{Re\cdot K}v, \tag{3}$$

$$u\frac{\partial C}{\partial x}+v\frac{\partial C}{\partial y}=\frac{1}{Re\cdot Sc}\left[\frac{\partial^2 C}{\partial x^2}+\frac{\partial^2 C}{\partial y^2}\right], \tag{4}$$

Where u,v,p,T and C act as the axial velocity, radial velocity, pressure, temperature and solute concentration components of the streaming blood, respectively. Meanwhile, the appropriate conditions are imposed at certain boundaries of the domain corresponding to a fully developed flows of a non-Newtonian fluid [24], a non-slip condition along the wall boundaries of the artery considering that the malfunction of wall motion occurs in a diseased artery [25] and a traction free condition on the outlet boundaries of the branch artery [16], respectively, given in non-dimensional form as,

$$u=\frac{3n+1}{n+1}\left(1-\left(\frac{y}{0.5}\right)^{\frac{(n+1)}{n}}\right), v=0, \text{ and } C=1 \text{ on } \Gamma_{inlet},$$

$$u=0, v=0, \text{ and } C=0 \text{ on } \Gamma_{wall},$$
$$(-p\mathbf{I}+\frac{\mu_a}{Re}\mathbf{D}(\mathbf{u}))\mathbf{n}=\mathbf{t}_h,\ (\frac{1}{Re\cdot Sc}\mathbf{D}(C))\mathbf{n}=\mathbf{t}_h \text{ on } \Gamma_{outlet}, \tag{5}$$
$$\text{where } \mathbf{D}=\frac{1}{2}\left(\nabla\boldsymbol{\omega}+(\nabla\boldsymbol{\omega})^T\right),\ \boldsymbol{\omega}=(u,v,C) \text{ and } \mathbf{t}_h=0.$$

Where $\Gamma_{inlet}, \Gamma_{wall}$ and Γ_{outlet} are the inlet, wall and outlet boundaries of the domain Ω, respectively. The unit outward normal vector, the vector of the prescribed boundary tractions, the unit tensor, and the strain rate tensor are exhibited by the respective parameters $\mathbf{n}, \mathbf{t}_h, \mathbf{I}$ and $\mathbf{D}$. The parameters μ_a, Re, M, K and Sc which appear due to the non-dimensionalization procedure represent the apparent viscosity for the power law fluid model, Reynolds number, Hartmann number, porosity constant and Schmidt number, respectively. These parameters are produced through a combination of several parameters for the simplification of physical dimensions involved in this model. Hence, these non-dimensional variables which appear in Eq. (1) – Eq. (4) could be defined as,

$$\mu_a=\frac{\bar{\mu}_a\bar{h}^{n-1}}{m\bar{u}_r^{n-1}}, Re=\frac{\rho\bar{u}_r^{2-n}\bar{h}^n}{m}, M=B_0\left(\frac{\sigma\bar{h}^{n+1}}{m\bar{u}_r^{n-1}}\right)^{\frac{1}{2}}, K=\frac{k}{\bar{h}^2}, Sc=\frac{m}{\rho D_m}\left(\frac{\bar{u}_r}{\bar{h}}\right)^{n-1}. \tag{6}$$

In Eq. (6), the diameter of the arterial's inlet is denoted by the characteristic length, $\bar{h}$, the fluid's consistency parameter is characterised as m, and the average mean inflow velocity is represented as $\bar{u}_r$. In addition, the parameters ρ, B_0, σ, k and D_m indicate the density of blood, intensity of magnetic flux, electrical conductivity of blood, constant coefficient which defines the porosity of the medium and constant coefficient of diffusion, respectively. Also, the viscosity function for the power law fluid model signified here as μ_a could be mathematically expressed as [26],

$$\mu_a=\left|(I_2)\right|^{\frac{(n-1)}{2}},\ I_2=2\left(\frac{\partial u}{\partial x}\right)^2+2\left(\frac{\partial v}{\partial y}\right)^2+\left(\left(\frac{\partial u}{\partial y}\right)^2+2\left(\frac{\partial v}{\partial x}\right)^2\right), \tag{7}$$

Where n is the power law index that is chosen following the condition of fluid characterisation and I_2 is the second invariant of the strain rate tensor. The non-dimensional variables involved in the transformation of governing equations obtained in Eq. (1) – Eq. (4) and boundary conditions acquired in Eq. (5) as a simplified non-dimensional system are as follows,

$$x=\frac{\bar{x}}{\bar{h}},\ y=\frac{\bar{y}}{\bar{h}},\ u=\frac{\bar{u}}{\bar{u}_r},\ v=\frac{\bar{v}}{\bar{u}_r},\ p=\frac{\bar{p}}{\rho\bar{u}_r^2},\ C=\frac{\bar{C}}{C_s}, \tag{8}$$

Where C_s stands as the reference concentration of solute at the arterial inlet, while the '¯' which appears in Eq. (8) on top of certain variables are indication of each physical quantity which exist in their dimensional form. To ease the numerical formulation which will be implemented in the

following section, the governing equations expressed in Eq. (1) – Eq. (4) with prescribed boundary conditions specified in Eq. (5) are written in a simplified vector form as follows,

$$
\begin{aligned}
&\nabla \cdot \mathbf{u} = 0 && \text{in } \Omega, \\
&\mathbf{u} \cdot \nabla \mathbf{u} - \frac{\mu_a}{\mathrm{Re}} \nabla \cdot \mathbf{D}(\mathbf{u}) + \nabla p = \mathbf{f} && \text{in } \Omega, \\
&\mathbf{u} \nabla C - \frac{1}{\mathrm{Re} \cdot Sc} \left(\nabla \cdot \mathbf{D}(C) \right) = 0 && \text{in } \Omega, \\
&\mathbf{u} = \mathbf{u}_g && \text{on } \Gamma_g, \\
&(-p\mathbf{I} + \frac{1}{\mathrm{Re}} 2\mu_a \mathbf{D}(\mathbf{u}))\mathbf{n} = \mathbf{t}_h && \text{on } \Gamma_{outlet}, \\
&(\frac{1}{Re \cdot Sc} \mathbf{D}(C))\mathbf{n} = \mathbf{t}_h && \text{on } \Gamma_{outlet},
\end{aligned}
\tag{9}
$$

Where $\mathbf{D} = \frac{1}{2}\left(\nabla \boldsymbol{\omega} + (\nabla \boldsymbol{\omega})^T \right)$, $\boldsymbol{\omega} = (u, v, C)$ and $\mathbf{t}_h = 0$. Γ_g indicates the boundary section, Γ of the domain Ω that is imposed by the Dirichlet boundary conditions. Referring to the body forces expressed in Eq. (2) and Eq. (3), the body force vector, $\mathbf{f}$ from Eq. (9) are then comprised as $(-\frac{M^2}{Re} u - \frac{1}{Re \cdot K} u, -\frac{1}{Re \cdot K} v)$. By the non-dimensionalisation procedure, the boundary configurations of the domain illustrated in Figure 1 are also being non-dimensionalised to a finite horizontal length of 6.333333 with vessel's inlet equivalent to 1.

3. Numerical Methodology

3.1 Galerkin Least-squares Method

The solutions for the boundary value problem for the system of equations specified in Eq. (1) - Eq. (4) subject to boundary conditions inflicted as Eq. (5) are approximated numerically by a stabilization technique of a finite element approach, known as the Galerkin least-squares method. Therefore, the degrees of freedom involved in this study are comprised of the components of velocity $(\mathbf{V}_h \text{ and } \mathbf{V}_g^h)$, pressure (P_h) and concentration of solute $(\mathbf{C}_h \text{ and } \mathbf{C}_g^h)$ which are approximated according to the finite element subspaces which are typically defined in fluid dynamics [27, 28] as,

$$
\begin{aligned}
&\mathbf{V}_h = \mathbf{C}_h = \left\{ \mathbf{N} \in \left[H_0^1(\Omega) \right]^{nsd} \mid \mathbf{N}_{|\mathrm{K}} \in R_k(\Omega_K)^{nsd},\ \Omega_K \in X_h \right\}, \\
&\mathbf{V}_h^g = \mathbf{C}_h^g = \left\{ \mathbf{N} \in \left[H^1(\Omega) \right]^{nsd} \mid \mathbf{N}_{|\mathrm{K}} \in R_k(\Omega_K)^{nsd},\ \Omega_K \in X_h,\ \mathbf{N} = \boldsymbol{\omega}_g \text{ on } \Gamma_g \right\}, \\
&P_h = \left\{ p \in C^0(\Omega) \cap L_0^2(\Omega) \mid q_{|\mathrm{K}} \in R_l(\Omega_K)^2,\ \Omega_K \in X_h \right\}.
\end{aligned}
\tag{10}
$$

The standard finite element spaces in Eq. (10) are defined over a partition X_h in a closed domain $\overline{\Omega}$ consisting of a triangular element $P_m(\Omega_K)$ with degree $m = 2$. Hence, the polynomial spaces for all components denoted as R_m are defined as $(m = k, l)$ corresponding to an equal degree of interpolation functions for $\mathbf{u}_h, p_h$ and C_h which are approximated by using a quadratic order of triangular element, P_2 / P_2. Also, the vector $\boldsymbol{\omega}_g$ describes the conditions for $\mathbf{u}, p$ and C which are prescribed over g boundaries of the domain. Based on the functional spaces defined in Eq. (10), the

Galerkin least-squares formulation for the non-linear boundary value problem introduced in Eq. (9) can be stated as to find the solutions of $\mathbf{u}_h \in \mathbf{V}_h$, $p_h \in P_h$ and $C_h \in \mathbf{C}_h$, given as

$$B(\mathbf{u}_h, p_h, C_h; \mathbf{N}, q, \mathbf{N}) = F(\mathbf{N}, q, \mathbf{N}),\ \forall (\mathbf{N}, q) \in (\mathbf{V}_h \times P_h), \tag{11}$$

where,

$$\begin{aligned} B(\mathbf{u}, p, C; \mathbf{N}, q, \mathbf{N}) &= \int_\Omega \mathbf{u}\nabla\mathbf{u}\cdot\mathbf{N}d\Omega + \int_\Omega \frac{1}{Re}\mathbf{D}(\mathbf{u})\cdot\mathbf{D}(\mathbf{N})d\Omega - \int_\Omega p\nabla\cdot\mathbf{N}d\Omega \\ &- \int_\Omega q\nabla\cdot\mathbf{u}d\Omega + \int_\Omega \mathbf{u}\nabla C\cdot\mathbf{N}d\Omega + \int_\Omega \frac{1}{Re\cdot}\mathbf{D}(C)\cdot\mathbf{D}(\mathbf{N})d\Omega \\ &+ \sum_{\Omega_{K\in C_h}} \int_{\Omega_K} \left[\begin{array}{l} \left(\mathbf{u}\nabla\mathbf{u} + \nabla p - \frac{1}{Re}\left(\nabla\cdot\mathbf{D}(\mathbf{u})\right)\right) \\ \cdot\left(\tau(Re_K)\right)\left(\mathbf{u}\nabla\mathbf{N} + \nabla q - \frac{1}{Re}\left(\nabla\cdot\mathbf{D}(\mathbf{N})\right)\right) \\ +\left(\mathbf{u}\nabla C - \frac{1}{Re\cdot Sc}\left(\nabla\cdot\mathbf{D}(C)\right)\right) \\ \cdot\left(\tau(Re_K)\right)\left(\mathbf{u}\nabla\mathbf{N} - \frac{1}{Re\cdot Sc}\left(\nabla\cdot\mathbf{D}(\mathbf{N})\right)\right) \end{array} \right] d\Omega_K, \end{aligned} \tag{12}$$

and

$$\begin{aligned} F(\mathbf{N}, q, \mathbf{N}) &= \int_\Omega \mathbf{f}\cdot\mathbf{N}d\Omega + \int_\Gamma \mathbf{t}_h\cdot\mathbf{N}d\Gamma \\ &+ \sum_{\Omega_{K\in C_h}} \int_{\Omega_K} \left[\mathbf{f}\cdot\left(\tau(\mathrm{Re}_K)\left(\mathbf{u}\nabla\mathbf{N} + \nabla q - \frac{1}{\mathrm{Re}}\left(\nabla\cdot\mathbf{D}(\mathbf{N})\right)\right)\right)\right] d\Omega_K. \end{aligned} \tag{13}$$

From the above formulation, it is worth noting here that the terms without the summation sign are originated from the weak formulation of a classical Galerkin method and the terms within the summation sign in Eq. (12) and Eq. (13) are the added stabilization terms which are obtained from the minimization of the functional residuals constructed from Eq. (9). The stabilization parameter, $\tau(Re_K)$ is adopted from the existing study performed by Franca and Madureira [29] which is applicable for the higher order element with degree $k \geq 2$. These added residual-based terms may be specified as [29],

$$\tau(\mathrm{Re}_K)=\frac{\xi(\mathrm{Re}_K)}{\sqrt{\lambda_K}\,|\mathbf{u}|_2},$$
$$\mathrm{Re}_K=\frac{|\mathbf{u}|_2}{4\sqrt{\lambda_K}\,\mu_a/\rho}\ \text{and}\ |\mathbf{u}|_2=\left(\sum_{i=1}^{2}|u_i|^2\right)^{1/2},$$
$$\xi(\mathrm{Re}_K)=\begin{cases}\mathrm{Re}_K, 0\le \mathrm{Re}_K<1\\ 1, \mathrm{Re}_K\ge 1\end{cases}, \tag{14}$$
$$\lambda_K \max_{0\neq\mathbf{N}\in(R_k(\Omega_K)/\square)^N}=\frac{\|\Delta\mathbf{N}\|^2_{0,\Omega_K}}{\|\nabla\mathbf{N}\|^2_{0,\Omega_K}},\Omega_K\in X_h,$$

Where the parameter λ_K is uniquely determined as the maximum eigenvalue for the generalized eigenvalue problem defined for each Ω_K following the associated problem designed and solved by Franca and Madureira [29] as well as Harari and Hughes [25] for the selected degree of polynomial $k.$, as to find $\{\lambda_K,\mathbf{N}\},\mathbf{N}\in R_k/\square(\Omega_K),$ such that

$$(\Delta\omega_h,\Delta\mathbf{N})-\lambda_K(\nabla\omega_h,\nabla\mathbf{N})=0,\ \forall\omega_h\in R_k/\square(\Omega_K). \tag{15}$$

To solve the set of coupled, non-linear, differential equations expressed in Eq. (11) – Eq. (13), the non-linear algebraic system is introduced by writing the equations in terms of the symbolic format of,

$$\mathbf{R(U)}=\overline{\mathbf{K}}\mathbf{(U)U}-\overline{\mathbf{F}}=0, \tag{16}$$

where $\mathbf{U}$ denotes vectors for the degrees of freedom of the associated problem that are spatially discretized with isoparametric triangle elements of quadratic order for the velocity, pressure and concentration components within an element, $e_i,i=1,2,3,....N_e$, given as

$$\mathbf{u}=\mathbf{u}^{e_i}=\mathbf{N}_j^{e_i}\mathbf{u}_j,$$
$$p=p^{e_i}=q_j^{e_i}p_j, \tag{17}$$
$$T=C^{e_i}=\mathbf{N}_j^{e_i}C_j,$$

Where N_e denotes the total number of elements, while $j=1,2,3,4,5,6$ correspond to three corner nodes and three centre nodes. Also, $\mathbf{R}$ stands as the nonlinear operator containing the vector components of the residuals function, $\overline{\mathbf{K}}$ is the stiffness matrix made up of the advective, diffusive, pressure, constraint of incompressible terms as well as terms generated from the added least squares formulation and $\overline{\mathbf{F}}$ represents the functions of body force and applied boundary conditions. In order to solve the above non-linear system, help from an iterative method is required to linearize the non-linear terms originating from the advection terms. Hence, for the above system, the algorithm for solving the equation set is given as,

$$\mathbf{R}(\mathbf{U}^b) = -\left.\frac{\partial \mathbf{R}}{\partial \mathbf{U}}\right|_{\mathbf{U}^b} \Delta\mathbf{U} \equiv -J(\mathbf{U}^b)\Delta\mathbf{U}, \tag{18}$$

Where $\Delta\mathbf{U} = (\mathbf{U}^{b+1} - \mathbf{U}^b)$. As specified in Eq. (17), $J(\mathbf{U}^b) = \left.\frac{\partial \mathbf{R}}{\partial \mathbf{U}}\right|_{\mathbf{U}^b}$ implies the Jacobian matrix, also recognized as tangent matrix, while the superscript b and $b+1$ acts as the iteration number. The solutions for the above system then are computed as,

$$\mathbf{U}^{b+1} = \mathbf{U}^b - J(\mathbf{U}^b)\mathbf{R}(\mathbf{U}^b). \tag{19}$$

The above relation is computed iteratively until the specific values of convergence tolerance, τ for the maximum residual norm, R_I is fulfilled. The convergence parameter may be calculated as

$$\tau \le \sqrt{\sum_{I=1}^{N} R_I^2}. \tag{20}$$

The computation of numerical integrals of Eq. (11) – Eq. (13) are carried out via the Gaussian quadrature technique. The essential steps for the algorithm are summarized as,

i. The Stokes solution for the Newtonian fluid flow $(b=1)$ is estimated as the initial guess for $\mathbf{U}^0$. The number of iterations, b is set.
ii. The Residuals matrix is constructed by using the initial guess $\mathbf{U}^0$, stiffness matrix, $\overline{\mathbf{K}}(\mathbf{U}^b)$ and body force matrix, $\overline{\mathbf{F}}(\mathbf{U}^b)$ which is constructed by using the Picard iteration method.
iii. The convergence tolerance, τ is computed as Eq. (20). If $\left|R_I(\mathbf{U}^{b+1})\right|_\infty > \tau$, then the Jacobian matrix, $J(\mathbf{U}^b)$ is computed by using Newton's method.
iv. The incremental vector, $\Delta\mathbf{U}$ then is computed as $(\mathbf{U}^{b+1} - \mathbf{U}^b)$.
v. The solutions vector is solved for $\mathbf{U}^{b+1}$.
vi. Repeat step 2-5 by using the updated solutions for the next iteration until the convergence criteria in step 3 is achieved. If the condition set for convergence tolerance is fulfilled, the solutions found are converged. The solutions for $\mathbf{U}^{b+1}$ are saved and the algorithm is completed.

In this study, finite element meshes are generated using the "mesh2d" function developed by Darren Engwirda for triangular elements, which is available online and can be downloaded from the MathWorks webpage (www.mathworks.com).

3.1 Algorithms Validation

In this section, a numerical validation on the source code that has been developed according to the Galerkin-least squares algorithm is performed to certify the applicability of the developed source code in computing the solutions of the system of Eq. (11) - Eq. (13). The verification is conducted with the existing studies of Bell and Surana [31] as well Ghia *et al.,* [32] which works on the respective flow of non-Newtonian power law model and Newtonian model in a lid-driven cavity. Fundamentally, the results on the u-velocity profile along the vertical centreline of the cavity for $Re = 100$ and $n = 1$ are

generated for several mesh distributions to publish a mesh-independent finding as shown in Figure 2. To achieve that, the results are generated by using five variations of finite element meshes consisting of 6856, 10328, 12076, 14396 and 17524 unstructured triangular elements. As presented in Figure 2, it is obvious that the mesh-independent results are obtained with a mesh design comprising 12076 unstructured triangular elements which is made up of 6239 nodes. The final optimized selected mesh is prescribed with a maximum element size of $h_{max} = 0.0115$, since modifying the element size beyond this design does not significantly alter the accuracy of the u-velocity profiles along the vertical centreline of the cavity.

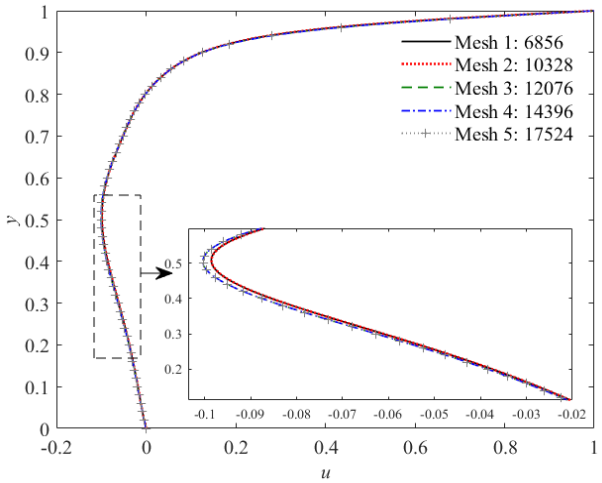

Fig. 2. Mesh independence test of u-velocity profiles along the vertical centreline of the cavity for $Re = 100$ and $n = 1$

The mesh design for the selected mesh is demonstrated in Figure 3 with the conditions prescribed over the boundaries of the domain.

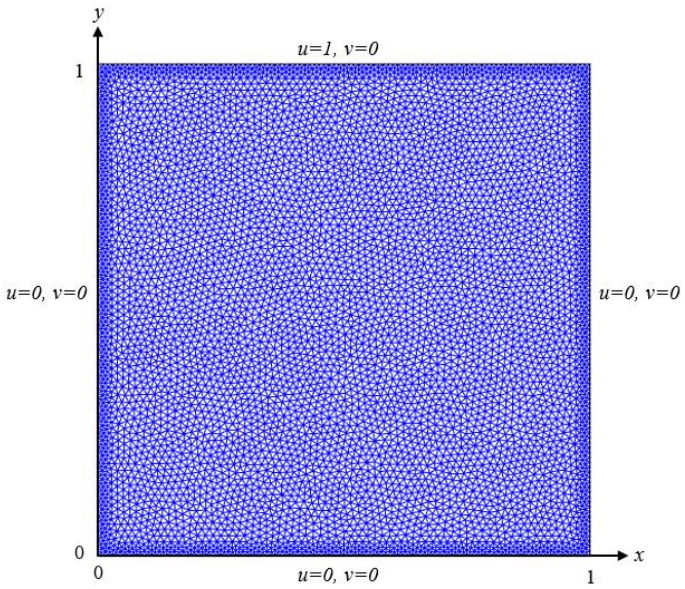

Fig. 3. The selected mesh for lid cavity problem with prescribed boundary conditions

Hence, by using the selected mesh, the benchmark analysis is then performed for the axial velocity distributions along the vertical mid line of the cavity for different fluid characterisations classified with varying power law index, n. The validity of the developed source code, which works according to the Galerkin least-squares algorithms summarised in the preceding sub-section, is declared here through the close correlation of findings obtained for the non-Newtonian power law model as well as Newtonian model with existing findings attained by Bell and Surana [31] and Ghia *et al.,* [32], respectively, as shown in Figure 4.

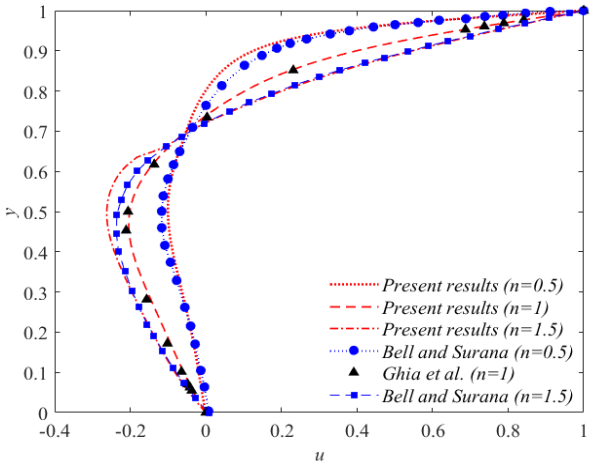

Fig. 4. Comparison of results on u-velocity profiles along the vertical centreline of the cavity obtained from this present study verified with existing results by Bell and Surana [31] for $n=0.5,1.5$ and Ghia *et al.,* [32] for $n=1$ at $Re=100$

4. Result and Discussion

4.1 Mesh Independence Test

A similar approach to accomplish a mesh independent solution in the last sub-section is carried out on the bifurcated channel by considering four different kinds of mesh design comprised of 10857, 14780, 17278 and 26814 domain elements across several locations of the branch artery. From the mesh independence analysis that is demonstrated, an appreciable difference between the results generated on u-velocity profiles are detected predominantly at the apex of the branch artery approximated for shear-thinning fluids nature, $n=0.5$ at $Re=300, Sc=0, M=2$ and $K=1$, as visualized in Figure 5.

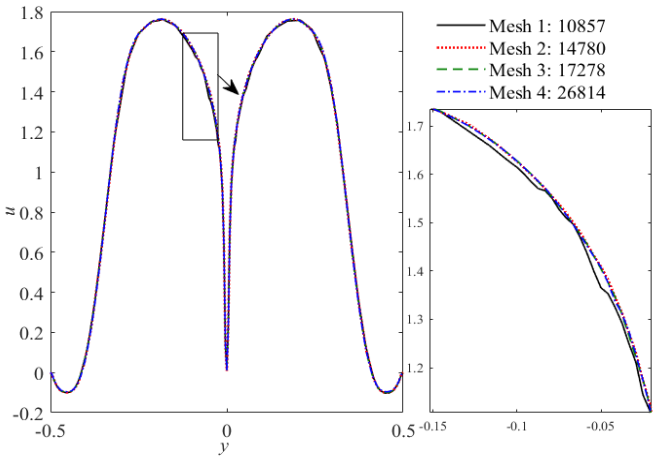

Fig. 5. Mesh independence test of u-velocity profiles at $x=3.345102$ (apex) location of the channel for $n=0.5, Re=300, Sc=0, M=2$ and $K=1$

It is clearly observed from the present figure that a smooth curve is developed for mesh 2, mesh 3 and mesh 4. In addition, the curves produced for these three consecutives meshes are in close correlation between one another with no significant difference spotted between the curves line as the element density is increased. Hence, the mesh independence results are attained by using the finite element mesh design consisted of 14780 unstructured triangular elements generated from 8283 nodes that is prescribed with a maximum element size of $h_{max}=0.065$, as presented in Figure 6. All simulations performed in this present study are approximated by the selected mesh 2 having quadratic order on each triangular element.

4.2 Hemodynamical Analysis of Blood Flow Simulation

Note that parameters involved in the considered problem must be assigned prior to further numerical computation. The Hartmann number M signifies the ratio of electromagnetic force to the viscous force that is considered as purely hydrodynamics, $M=0$ as well as purely magnetohydrodynamics, $M=2,4$ when the system is influenced respectively by no magnetic source, $B_0=0\mathrm{T}$ and strong magnetic field of strength, $B_0=8.819171\mathrm{T}, 17.638342\mathrm{T}$ with the blood electrical conductivity, $\sigma=0.8\mathrm{S/m}$ and the blood density, $\rho=1050\mathrm{kg/m}^3$. The enhancement in permeability of the porous medium is represented by increasing value of parameters $K=0,1,2$. The main aim of this work is to simulate the mass transport phenomena of the non-Newtonian power law fluid flow that is affected by the magnetic source application, M and flow porosity, K. The non-Newtonian nature of blood is described as shear-thinning, Newtonian and shear-thickening fluids corresponding to varying values of power law index indicated as $n=0.6$ $(n<1)$, $n=1$, and $n=1.4$ $(n>1)$, with fluid's consistency parameter varied as $m=0.006356, 0.0035, 0.001927$, respectively, for fixed value of average inflow velocity, $\bar{u}_r=6.666667\times10^{-2}\mathrm{m/s}$ obtained for Reynolds number, $Re=300$. Meanwhile, for constant coefficient of diffusion, $D_m=6.666666\times10^{-6}\mathrm{m}^2/\mathrm{s}$, the Schmidt number then is calculated as $Sc=0.5$. The solutions for the considered problem act in a satisfied manner with a convergence tolerance set in an order of $\tau=10^{-6}$ and by using these sets of parameters to construct the arterial geometry of the branch artery: $a=0.5$, $l_0=1.333333$, $d=1$, $x_{max}=6.333333$, $x_1=3$, $q=0.013333$, $\beta=30^{\circ}$, $r_1=0.51a$ and $\bar{h}=0.015\mathrm{m}$.

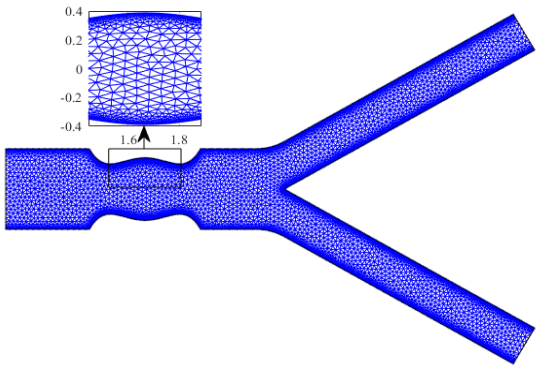

Fig. 6. The optimized selected mesh for the present GLS algorithms simulation of unstructured triangular element

The distribution of non-dimensional variables of velocity and shear stress are simulated graphically in terms of filled contour by varying the values of flow porosity, K and magnetic source, M for different kinds of fluid characterisation, n as depicted in Figure 7 – Figure 10 at fixed values of Reynolds and Schmidt numbers, $Re = 300, Sc = 0.5$. Apparently, the increment in flow porosity has led to a reduction in the maximum velocity that is developed in the constricted area with intangible changes in flow recirculation formed at the downstream region of stenosis in spite of an elevation in K from $K = 0$ to $K = 2$. This flow pattern could result from the enhancement of fluid motion driven by the decreased resistance of blood flow as the flow porosity increases [19]. As the power law index is increased from $n = 0.6$ to $n = 1.4$, the maximum velocity which is developed in the area of constriction has increased significantly. The obstructed area caused by the formation of stenosis has hindered the flow of blood while approaching this area, the fluids flow is accelerated to keep the blood circulation across this region. Therefore, the shear-thickening fluid attains the highest maximum velocity around the constricted area compared to its counterparts. This is due to its fluid viscosity, which is much lower in the low shear rate region compared to the Newtonian and shear-thinning fluids. As a result, the shear-thickening fluid flows at a higher velocity through the constricted region compared to its counterparts. The velocity across the daughter branches for $n = 1.4$ are the most declined in magnitudes based on the filled contour of velocity visualized in Figure 7 compared to the other fluid characterisations. These fluid behaviours correspond to changes in the apparent viscosity of fluids according to different power law indices. This enables the shear-thinning fluid to flow more easily (with less resistance) compared to fluids characterized by Newtonian and shear-thickening behaviour. Conversely, the shear-thickening fluid exhibits a more resistive motion of fluid in accordance with its viscosity, which increases with the shear rate.

On the other hand, the notable influence of magnetic fields is discovered for the distributions of velocity contour and vortex formation, which are both diminished in magnitude and size, respectively, as the magnetic sources are magnified from $M = 0$ to $M = 4$. The increment in magnetic field intensities obviously lead to the enhancement of hydro magnetic Lorentzian drag force that has a tendency to oppose the fluid particles and diminishes the blood flow motion. As illustrated in Figure 8, shear-thinning fluid, $n = 0.6$ is the fluid characterisation that is less viscous in comparison to its counterpart, which is Newtonian, $n = 1$ and shear-thickening fluid, $n = 1.4$, possesses the highest magnitude of velocity passing through the arterial branches with the least maximum velocity developed in the stenotic region. Therefore, the size of vortex formation is decreasing as the power

law index is increased from $n=0.6$ to $n=1.4$, which is in agreement with previous findings obtained by Halifi *et al.,* [26]. Among these three fluids, the shear-thinning fluid moves faster and possesses higher momentum. It is resistant for the same fluid layer to remain attached to suddenly changing geometry, thus exhibiting a more predominant vortex along the outer wall.

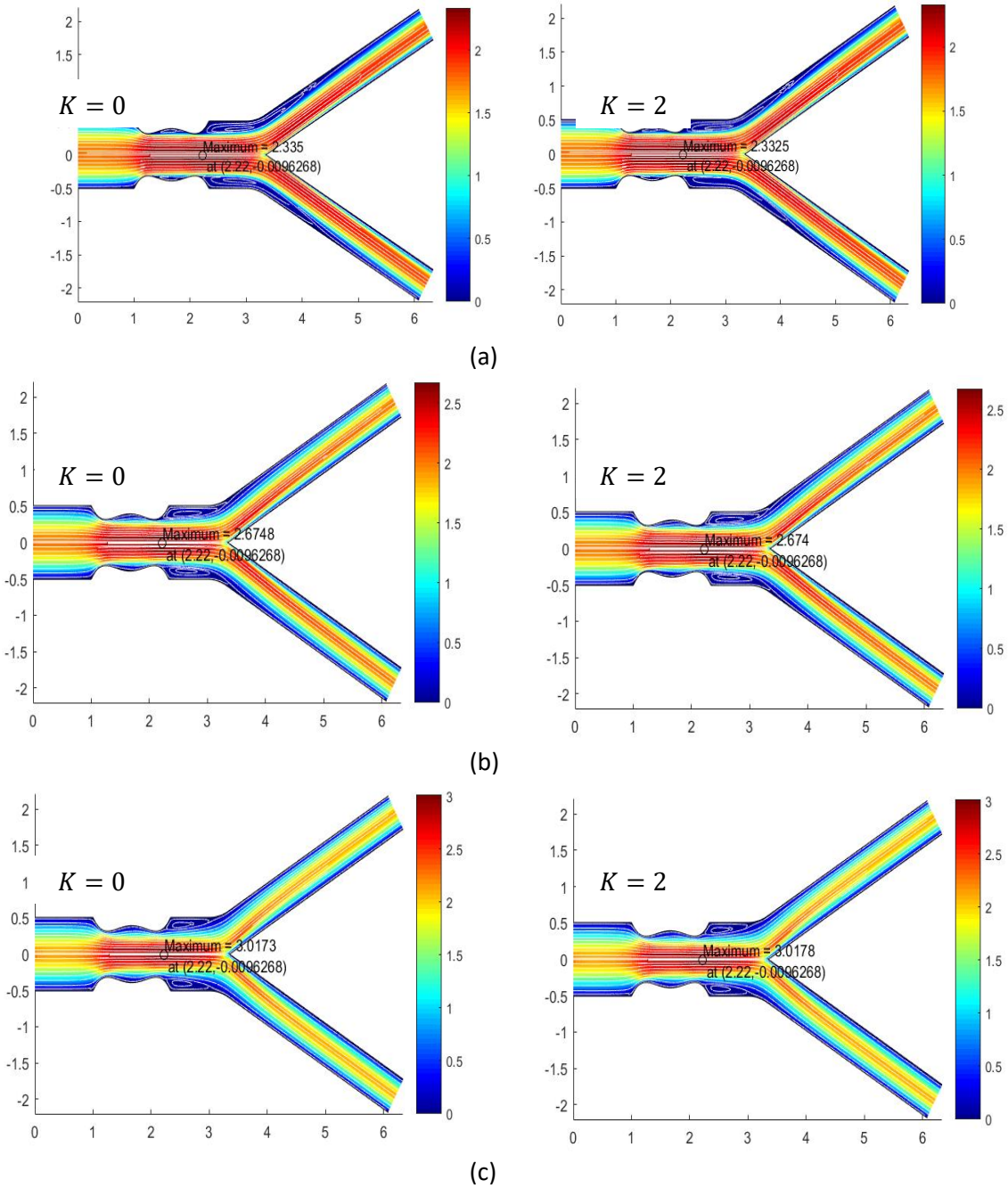

Fig. 7. Velocity contour and streamline pattern at various values of power law index, n and porosity constant, K for $Re=300, Sc=0.5$ and $M=2$ (a) $n=0.6$ (Shear-thinning) (b) $n=1$ (Newtonian)

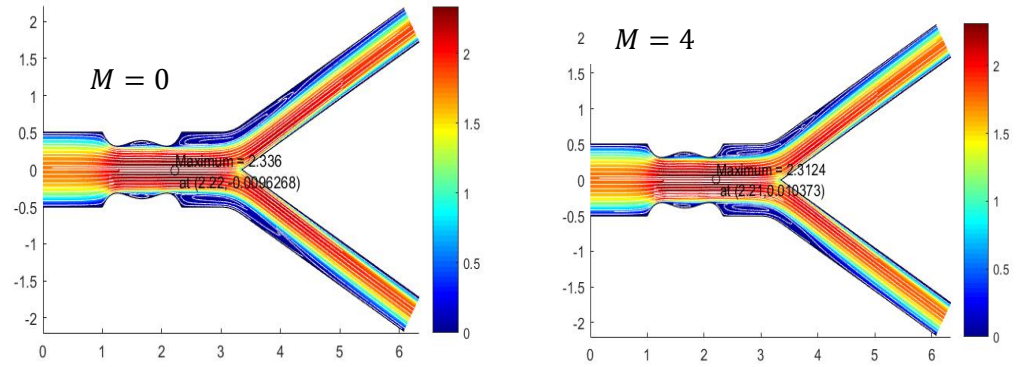

(a)

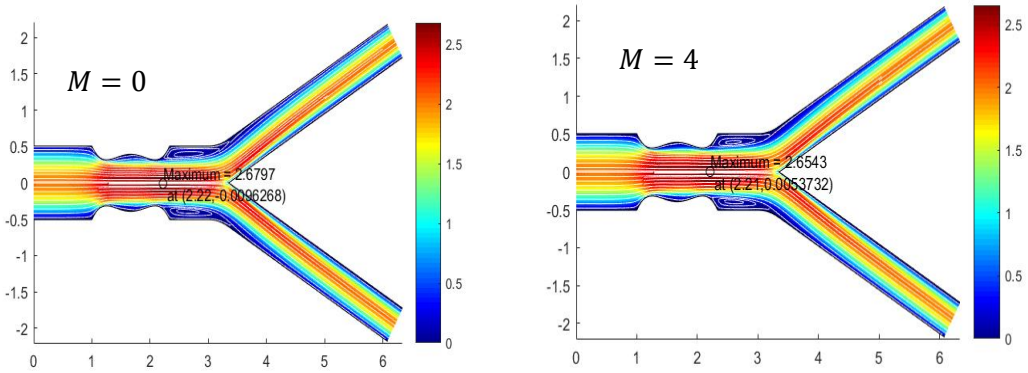

(b)

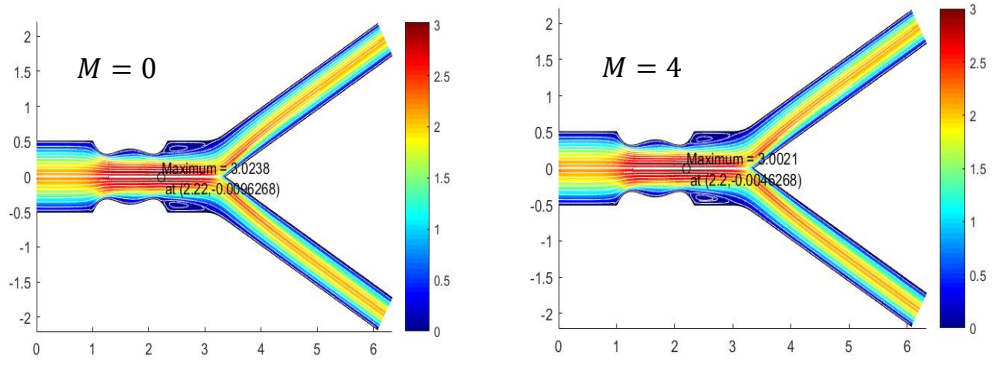

(c)

Fig. 8. Velocity contour and streamline pattern at various values of power law index, n and magnetic number, M for $Re = 300, Sc = 0.5$ and $K = 1$ (a) $n = 0.6$ (Shear-thinning) (b) $n = 1$ (Newtonian) (C) $n = 1.4$ (Shear-thickening)

Shear stress is a tangential shear force driven from the friction that is exerted by the blood on the arterial wall resulting from the fluids viscous nature [33, 34]. The assessment on shear stress distribution is clinically essential to gain knowledge on the local hemodynamic environment of coronary atherosclerosis, to identify a high-risk plaque as well as to examine the sites prone to plaque accumulation and its further atherosclerotic lesion progression [33]. As revealed in Figure 9 and Figure 10, a higher shear stress is observed at the throats of the stenosis and the apex of the branch artery irrespective of differences in fluid nature for varying effects of permeability of the porous medium, K and magnetic sources application, M,respectively. A large shear stress value corresponding to a large shear rate value promotes a high concentration of platelet near the vessel wall to assist in clotting and wound healing [35]. Meanwhile, the other regions in the arterial bifurcation seem to have a low shear stress value. Precisely, the lowest shear stress values are found around the axis of symmetry located at the parent's artery and downstream of stenosis where the flow separation region are identified as established in Figure 7 and Figure 8. A low shear stress value which developed at the downstream region of stenosis may promote the fat deposition to extend its size into the lumen of the side branch [36]. In fact, a low shear stress may turn a stable lesion into a high-risk plaque [37]. A constant exposure to a low shear stress value leads to a higher risk of plaque growth extended at the rear end of stenosis resulting in a severe stenotic condition. Clinically, the low shear stress pattern which may induce the inflammatory endothelial cells and a coupled effect of high LDL concentration would promote the growth of atherosclerosis [37]. The equivalent trends are observed on the increasing shear stress pattern as flow porosity, K as well as magnetic source, M intensifies, which suggests the idea of regulating the blood flow rates with a sufficient level of magnetic application and permeability of the porous media in a surgical procedure.

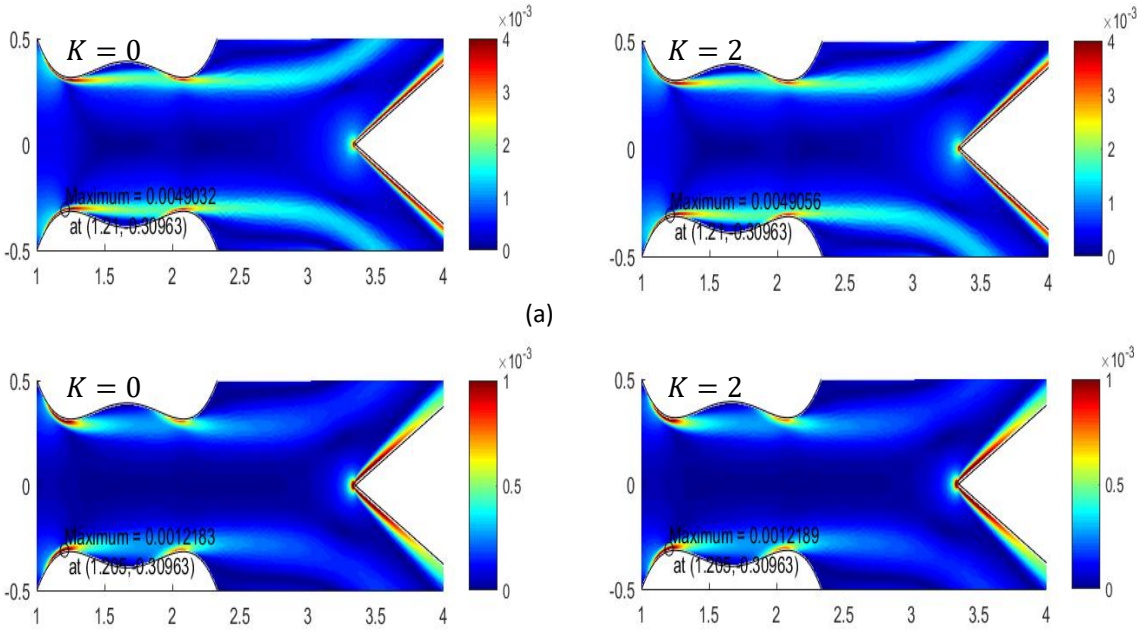

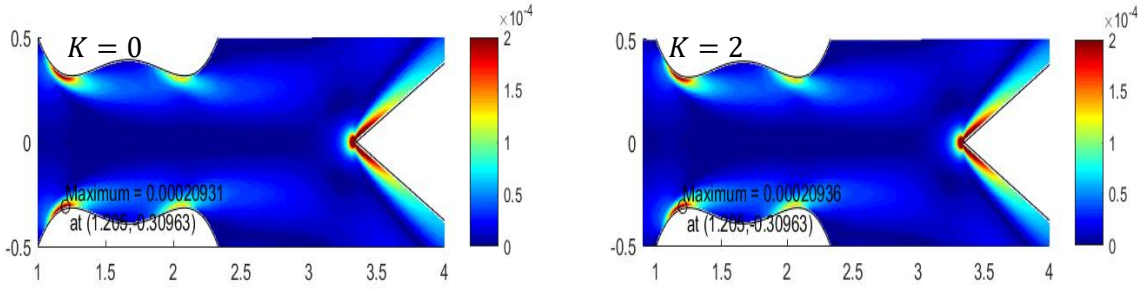

(c)

Fig. 9. Shear stress distribution at various values of power law index, n and porosity constant, K around the stenosis and apex of the branch artery for $Re = 300, Sc = 0.5$ and $M = 2$ (a) $n = 0.6$ (Shear-thinning) (b) $n = 1$ (Newtonian) (c) $n = 1.4$ (Shear-thickening)

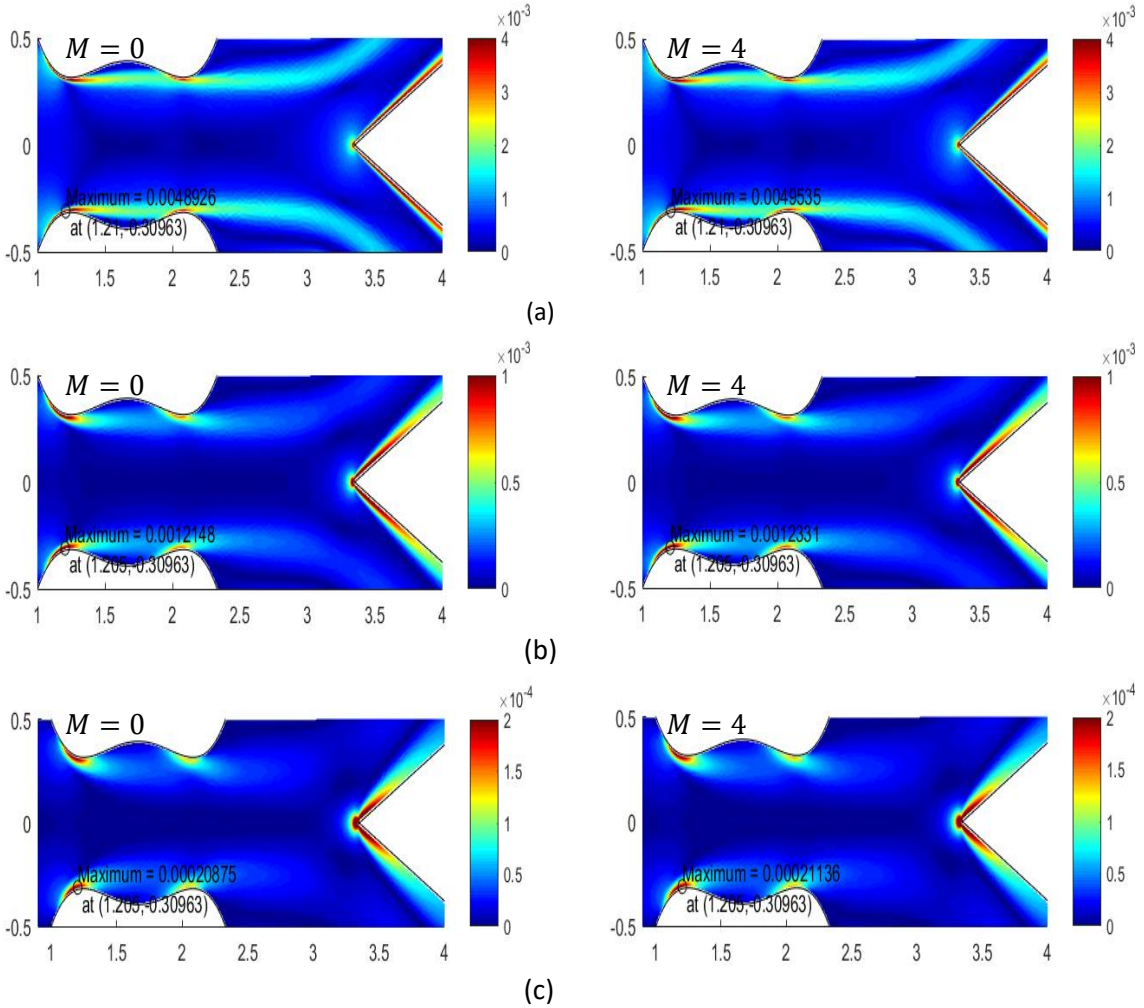

(a)

(b)

(c)

Fig. 10. Shear stress distribution at various values of power law index, n and magnetic number, M around the stenosis and apex of the branch artery for $Re = 300, Sc = 0.5$ and $K = 1$ (a) $n = 0.6$ (Shear-thinning) (b) $n = 1$ (Newtonian) (c) $n = 1.4$ (Shear-thickening)

The quantitative analysis on the mass transfer patterns that take place in three different fluid classifications through a stenosed arterial bifurcation are examined for varying effects of permeability of the porous media, K and magnetic source application, M as exhibited in Figure 11 and Figure 12 for $Re = 300$ and $Sc = 0.5$ in terms of the local Sherwood number distributions, computed mathematically as [3,4],

$$Sh_D = \frac{j_m \bar{h}}{D_m \Delta C}, \tag{21}$$

Where j_m the local is mass flux to the arterial wall and ΔC is a reference concentration difference that is evaluated as the difference between the concentration at the arterial inlet and the concentration at the arterial wall.

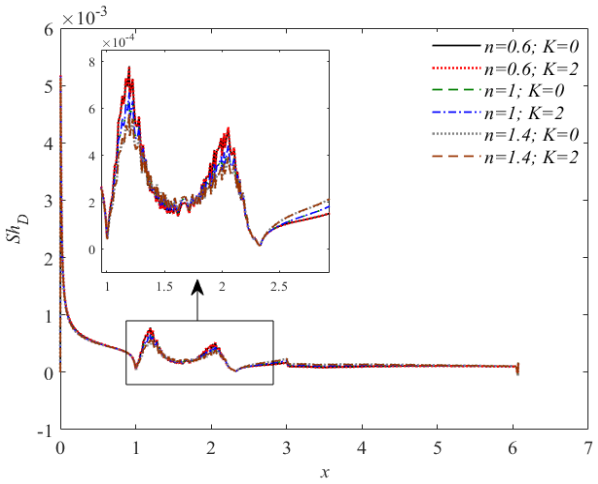

Fig. 11. Sherwood number distribution along the outer arterial wall at various values of power law index, n and porosity constant, K for $Re = 300, Sc = 0.5$ and $M = 2$

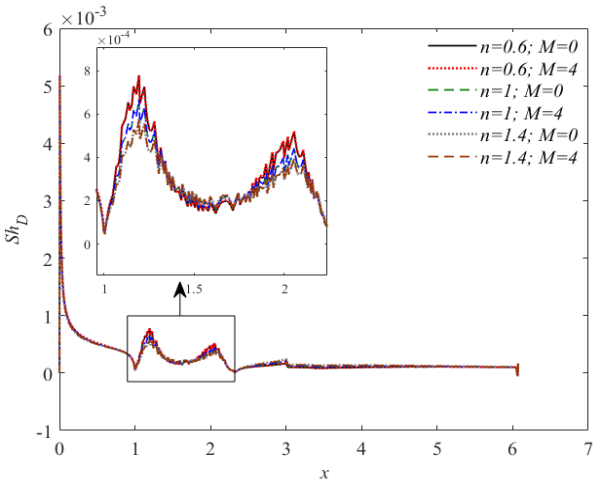

Fig. 12. Sherwood number distribution along the outer arterial wall at various values of power law index, n and Hartmann number, M for $Re = 300, Sc = 0.5$ and $K = 1$

The important features that may be observed from the two present figures are on a similar pattern of the Sh_D distribution obtained from the inlet to the onset of stenosis irrespective of the variation in fluid natures (n), magnetic sources (M) and flow porosity (K). A disparity in the Sh_D distribution is developed primarily at the constricted region where two peak values of mass transfer rate have developed prior to reaching the first throat of stenosis before passing through the second

throat of stenosis where fluids with increasing values of power law index, $n = 0.6,1,1.4$ contributed to the rising magnitudes of Sh_D. Apparent findings from Figure 11 and Figure 12 reported on the Sh_D distributions dropped significantly to the lowest magnitude at the offset of stenosis where the negative flow velocity has initiated and caused steep concentration gradients. The lowest mass transfer experienced at the downstream region of stenosis may enhance the cholesterol deposition at this region leading to a severe stenosis. While approaching the lateral junction of the daughter branch the magnitudes of Sh_D has slightly reduced and remains almost consistent throughout the non-constricted region of the branch artery. The effects of enhancing the permeability of the porous medium, K as well as the magnetic intensity, M is not salient in these present figures; somehow a slight reduction on the magnitudes of Sh_D are captured along with the increment of these two parameters. Hence, from this assessment, it is concluded that the streaming blood which behaves as a shear-thinning fluid accompanied by the greatest flow porosity and magnetic source application are more feasible to extend the accumulation of cholesterol at the downstream region of stenosis due to the distortions of local luminal mass transfer experienced by the shear-thinning fluid which possess the longest flow separated region in comparison to its counterpart.

4. Conclusions

A mathematical model on the hemodynamic of non-Newtonian power law model of blood flow influenced by the permeability of the porous medium and magnetic source application has been developed in relation to the mass transport mechanisms through an arterial segment having a constriction located at the parent artery in the shape of overlapping. The impacts of different fluid classifications are examined for $n = 0.6$ (shear-thinning), $n = 1$ (Newtonian), $n = 1.4$ (shear-thickening) concurrently with the variation in increasing magnetic intensities $(M = 0,4)$ and flow porosities $(K = 0,2)$ on the study of the velocity contours, streamline, shear-stress contours and the diffusive flux of the solute concentration. A close correlation achieved with previous numerical investigation has proved the applicability of the developed algorithms that work according to the Galerkin least-squares method as an effective method for simulating a purely viscous flow of non-Newtonian fluid through a complex arterial geometry coupled with the mass transport mechanisms in an arterial segment. The prominent findings acquired from this present investigation are:

i. Recirculation region (negative flow area) decreases for increasing values of power law index (n) and magnetic intensity (M).
ii. The effects of enhancing the permeability of the porous media (K) to the vortex formation is relatively negligible.
iii. Shear stress increases when flow porosity (K) and magnetic intensity (M) increases.
iv. Increasing the values of power law index (n) increases the shear stress.
v. The highest shear stress values are attained at the throat of an overlapping stenosis and around the apex of the arterial bifurcation for shear-thinning $(n = 0.6)$, Newtonian $(n = 1)$ and shear-thickening $(n = 1.4)$ fluids idealization.
vi. Sh_D distribution slightly decreases for increasing values of flow porosity (K) and magnetic intensity (M).
vii. Increasing values of power law index (n) increases the Sh_D distributions.

Based on the quantitative analysis conducted for the mass transfer and shear stress distributions of magnetohydrodynamics non-Newtonian power law flow of blood through a porous stenosed bifurcated artery, it can be inferred that streaming blood, behaving as a shear-thinning fluid, along with the greatest flow porosity and magnetic source application, is more likely to exacerbate the accumulation of cholesterol at the downstream region of stenosis. This is attributed to the distortions of local luminal mass transfer experienced by the shear-thinning fluid, resulting in the longest flow separated region compared to its counterpart. Additionally, with the highest magnitude of shear stress attained at the throat of stenosis, the shear-thinning fluid is implicated in endothelial detachment and platelet adhesion, thereby inducing thrombotic occlusion without rupture [30].

Acknowledgement
This research was funded by a grant from Research Management Centre, Universiti Teknologi Malaysia (UTM) under UTMShine grant 09G88.

References

[1] Schade, David S., Deborah Helitzer, and Philip Eaton. "Evidence that low density lipoprotein is the primary cause of atherosclerotic cardiovascular disease: a Bradford-Hill approach." *World Journal of Cardiovascular Diseases* 7, no. 9 (2017): 271-284.

[2] Liu, Yadong, and Wenjun Liu. "Blood flow analysis in tapered stenosed arteries with the influence of heat and mass transfer." *Journal of Applied Mathematics and Computing* 63, no. 1 (2020): 523-541. https://doi.org/10.1007/s12190-020-01328-5

[3] Alsemiry, Reima D., Prashanta K. Mandal, Hamed M. Sayed, and Norsarahaida Amin. "Numerical solution of blood flow and mass transport in an elastic tube with multiple stenoses." *BioMed research international* 2020 (2020). https://doi.org/10.1155/2020/7609562

[4] Sarifuddin, Santabrata Chakravarty, Prashanta Kumar Mandal, and Helge I. Andersson. "Mass transfer to blood flowing through arterial stenosis." *Zeitschrift für angewandte Mathematik und Physik* 60 (2009): 299-323. https://doi.org/10.1007/s00033-008-7094-2

[5] Mwapinga, Annord, Eunice Mureithi, James Makungu, and Verdiana Masanja. "Non-Newtonian heat and mass transfer on MHD blood flow through a stenosed artery in the presence of body exercise and chemical reaction." *Commun. Math. Biol. Neurosci.* 2020 (2020): Article-ID.https://doi.org/10.28919/cmbn/4906

[6] Amos, E., E. Omamoke, and Chinedu Nwaigwe. "Chemical reaction, heat source and slip effects on MHD pulsatory blood flowing past an inclined stenosed artery influenced by body acceleration." *International Journal of Mathematics Trends and Technology-IJMTT* 68 (2022).

[7] Chakravarty, Santabrata, and Subir Sen. "Dynamic response of heat and mass transfer in blood flow through stenosed bifurcated arteries." *Korea-Australia Rheology Journal* 17, no. 2 (2005): 47-62.

[8] Iasiello, Marcello, Kambiz Vafai, Assunta Andreozzi, and Nicola Bianco. "Analysis of non-Newtonian effects on low-density lipoprotein accumulation in an artery." *Journal of biomechanics* 49, no. 9 (2016): 1437-1446. doi: 10.1016/j.jbiomech.2016.03.017

[9] Hossain, Khan Enaet, and Md Mohidul Haque. "Influence of magnetic field on chemically reactive blood flow through stenosed bifurcated arteries." In *AIP Conference Proceedings*, vol. 1851, no. 1. AIP Publishing, 2017.doi: 10.1063/1.4984641

[10] Kumar, Devendra, B. Satyanarayana, Rajesh Kumar, Sanjeev Kumar, and Narendra Deo. "Application of heat source and chemical reaction in MHD blood flow through permeable bifurcated arteries with inclined magnetic field in tumor treatments." *Results in Applied Mathematics* 10 (2021): 100151. https://doi.org/10.1016/j.rinam.2021.100151

[11] Thirunanasambantham, Kannigah, Zuhaila Ismail, Lim Yeou Jiann, and Amnani Shamjuddin. "Numerical Computational of Blood Flow and Mass Transport in Stenosed Bifurcated Artery." *Journal of Advanced Research in Fluid Mechanics and Thermal Sciences* 110, no. 2 (2023): 79-94. https://doi.org/10.37934/arfmts.110.2.7994

[12] Khan, Ansab Azam, Khairy Zaimi, Suliadi Firdaus Sufahani, and Mohammad Ferdows. "MHD Flow and Heat Transfer of Double Stratified Micropolar Fluid over a Vertical Permeable Shrinking/Stretching Sheet with Chemical Reaction and Heat Source." *Journal of Advanced Research in Applied Sciences and Engineering Technology* 21, no. 1 (2020):1-14. https://doi.org/10.37934/araset.21.1.114

[13] Misra, J. C., A. Sinha, and G. C. Shit. "Mathematical modeling of blood flow in a porous vessel having double stenoses in the presence of an external magnetic field." *International Journal of Biomathematics* 4, no. 02 (2011): 207-225.

[14] Sinha, A., J. C. Misra, and G. C. Shit. "Effect of heat transfer on unsteady MHD flow of blood in a permeable vessel in the presence of non-uniform heat source." *Alexandria Engineering Journal* 55, no. 3 (2016): 2023-2033. https://doi.org/10.1016/j.aej.2016.07.010

[15] Sankar, A.R., Gunakala, S.R., Comissiong, D.M.G., Gunakala, S.R., and Comissiong, D.M.G. "Two-layered Blood Flow through a Composite Stenosis in the Presence of a Magnetic Field." *International Journal of Application or Innovation in Engineering & Management (IJAIEM)* 2, no. 12 (2013): 30-41.

[16] Saket, R. K., and Anil Kumar. "Reliability of Convective Diffusion Process in Stenosis Blood Vessels." *Chemical product and process modeling* 3, no. 1 (2008). https://doi.org/10.2202/1934-2659.1175

[17] Nandal, J., S. Kumari, and R. Rathee. "The effect of slip velocity on unsteady peristalsis MHD blood flow through a constricted artery experiencing body acceleration." *International Journal of Applied Mechanics and Engineering* 24, no. 3 (2019): 645-659. https://doi.org/10.2478/ijame-2019-0040

[18] Nadeem, S., Noreen Sher Akbar, T. Hayat, and Awatif A. Hendi. "Influence of heat and mass transfer on Newtonian biomagnetic fluid of blood flow through a tapered porous arteries with a stenosis." *Transport in porous media* 91 (2012): 81-100. https://doi.org/10.1007/s11242-011-9834-6

[19] Omar, Nur Fatihah Mod, Husna Izzati Osman, Ahmad Qushairi Mohamad, Rahimah Jusoh, and Zulkhibri Ismail. "Analytical solution of unsteady MHD casson fluid with thermal radiation and chemical reaction in porous medium." *Journal of Advanced Research in Applied Sciences and Engineering Technology* 29, no. 2 (2023): 185-194. https://doi.org/10.37934/araset.29.2.185194

[20] Omamoke, Ekakitie, and Emeka, Amos. "Chemical Reaction, Radiation and Heat Source Effects on Unsteady MHD Blood Flow Over a Horizontal Porous Surface in the Presence of an Inclined Magnetic Field." *International Journal of Scientific & Engineering Research* 11, no. 4 (2020): 1187-1192.

[21] Abdullahi, Isah, A. A. Hussaini, Domven Lohcwat, Ali Musa, and Mohammed Adamu. "Influence of Chemical Reaction, Heat Source and Thermal radiation on MHD Blood flow through a Porous Medium with an Inclined Magnetic field in Treatments of Cardiovascular Diseases." *GSJ* 10, no. 3 (2022).

[22] Chakravarty, Santabrata, and Prashanta Kumar Mandal. "An analysis of pulsatile flow in a model aortic bifurcation." *International journal of engineering science* 35, no. 4 (1997): 409-422. https://doi.org/10.1016/S0020-7225(96)00081-X

[23] Chakravarty, S., and P. K. Mandal. "Mathematical modelling of blood flow through an overlapping arterial stenosis." *Mathematical and computer modelling* 19, no. 1 (1994): 59-70.https://doi.org/10.1016/0895-7177(94)90116-3

[24] Husain, Iqbal, Fotini Labropulu, Chris Langdon, and Justin Schwark. "A comparison of Newtonian and non-Newtonian models for pulsatile blood flow simulations." *Journal of the Mechanical Behaviour of Materials* 21, no. 5-6 (2013): 147-153. https://doi.org/10.1515/jmbm-2013-0001

[25] Sousa, Luisa, C. A. T. A. R. I. N. A. Castro, C. A. R. L. O. S. Antonio, and R. Chaves. "Computational techniques and validation of blood flow simulation." *WEAS Transactions on biology and biomedicine, ISI/SCI Web of Science and Web of Knowledge* 8, no. 04 (2011): 145-155.

[26] Halifi, Adrian S., Sharidan Shafie, and Norsarahaida S. Amin. "Numerical solution of biomagnetic power-law fluid flow and heat transfer in a channel." *Symmetry* 12, no. 12 (2020): 1959. https://doi.org/10.3390/sym12121959

[27] Zinani, Flávia, and Sérgio Frey. "Galerkin least-squares solutions for purely viscous flows of shear-thinning fluids and regularized yield stress fluids." *Journal of the Brazilian Society of Mechanical Sciences and Engineering* 29 (2007): 432-443. https://doi.org/10.1590/S1678-58782007000400012

[28] Machado, Fernando, Flávia Zinani, and Sérgio Frey. "Herschel-Bulkley Fluid Flows Through a Sudden Axisymmetric Expansion via Galerkin Least-Squares Methodology." (2007).

[29] Franca, Leopoldo P., and Alexandre L. Madureira. "Element diameter free stability parameters for stabilized methods applied to fluids." *Computer methods in applied mechanics and engineering* 105, no. 3 (1993): 395-403. https://doi.org/10.1016/0045-7825(93)90065-6

[30] Harari, Isaac, and Thomas JR Hughes. "What are C and h?: Inequalities for the analysis and design of finite element methods." *Computer methods in applied mechanics and engineering* 97, no. 2 (1992): 157-192. https://doi.org/10.1016/0045-7825(92)90162-D

[31] Bell, Brent C., and Karan S. Surana. "p-version least squares finite element formulation for two-dimensional, incompressible, non-Newtonian isothermal and non-isothermal fluid flow." *International journal for numerical methods in fluids* 18, no. 2 (1994): 127-162. https://doi.org/10.1002/fld.1650180202

[32] Ghia, U. K. N. G., Kirti N. Ghia, and C. T. Shin. "High-Re solutions for incompressible flow using the Navier-Stokes equations and a multigrid method." *Journal of computational physics* 48, no. 3 (1982): 387-411. https://doi.org/10.1016/0021-9991(82)90058-4

[33] Papafaklis, Michail I., and Lampros K. Michalis. "Intravascular Imaging and Haemodynamics: The Role of Shear Stress in Atherosclerosis and In-Stent Restenosis." In *Intravascular Imaging: Current Applications and Research Developments*, pp. 326-348. IGI Global, 2012. https://doi.org/10.4018/978-1-61350-095-8.ch019

[34] Abdelwahab, A. M., Kh S. Mekheimer, Khalid K. Ali, A. El-Kholy, and N. S. Sweed. "Numerical simulation of electroosmotic force on micropolar pulsatile bloodstream through aneurysm and stenosis of carotid." *Waves in Random and Complex Media* (2021): 1-32. https://doi.org/10.1080/17455030.2021.1989517

[35] Weddell, Jared C., JaeHyuk Kwack, P. I. Imoukhuede, and Arif Masud. "Hemodynamic analysis in an idealized artery tree: differences in wall shear stress between Newtonian and non-Newtonian blood models." *PloS one* 10, no. 4 (2015): e0124575. https://doi.org/10.1371/journal.pone.0124575

[36] Song, Jianfei, Smaine Kouidri, and Farid Bakir. "Numerical study of hemodynamic and diagnostic parameters affected by stenosis in bifurcated artery." *Computer Methods in Biomechanics and Biomedical Engineering* 23, no. 12 (2020): 894-905.

[37] Arzani, Amirhossein. "Coronary artery plaque growth: A two-way coupled shear stress–driven model." *International journal for numerical methods in biomedical engineering* 36, no. 1 (2020): e3293.